12-22-2010

Propulsive Force Measurements and Flow Behavior of Undulatory Swimmers at Low Reynolds Number

Josué Sznitman
University of Pennsylvania

Xiaoning Shen
University of Pennsylvania, shenx@seas.upenn.edu

Raphael Sznitman
Johns Hopkins University

Paulo E. Arratia
University of Pennsylvania, parratia@seas.upenn.edu

Suggested Citation:
J. Sznitman, X. Shen, R. Sznitman and P.E. Arratia. (2010). "Propulsive force measurements and flow behavior of undulatory swimmers at low Reynolds number." *Physics of Fluids* **22**, 121901.

Propulsive Force Measurements and Flow Behavior of Undulatory Swimmers at Low Reynolds Number

Abstract
The swimming behavior of the nematode *Caenorhabditis elegans* is investigated in aqueous solutions of increasing viscosity. Detailed flow dynamics associated with the nematode's swimming motion as well as propulsive force and power are obtained using particle tracking and velocimetry methods. We find that *C. elegans* delivers propulsive thrusts on the order of a few nanonewtons. Such findings are supported by values obtained using resistive force theory; the ratio of normal to tangential drag coefficients is estimated to be approximately 1.4. Over the range of solutions investigated here, the flow properties remain largely independent of viscosity. Velocity magnitudes of the flow away from the nematode body decay rapidly within less than a body length and collapse onto a single master curve. Overall, our findings support that *C. elegans* is an attractive living model to study the coupling between small-scale propulsion and low Reynolds number hydrodynamics.

Disciplines
Engineering | Mechanical Engineering

Comments
Suggested Citation:
J. Sznitman, X. Shen, R. Sznitman and P.E. Arratia. (2010). "Propulsive force measurements and flow behavior of undulatory swimmers at low Reynolds number." *Physics of Fluids* **22**, 121901.

Propulsive force measurements and flow behavior of undulatory swimmers at low Reynolds number

J. Sznitman,[1,a)] X. Shen,[1] R. Sznitman,[2] and P. E. Arratia[1,b)]
[1]*Department of Mechanical Engineering and Applied Mechanics, University of Pennsylvania, Philadelphia, Pennsylvania 19104, USA*
[2]*Department of Computer Science, Johns Hopkins University, Baltimore, Maryland 2128, USA*

(Received 18 June 2010; accepted 30 November 2010; published online 22 December 2010)

The swimming behavior of the nematode *Caenorhabditis elegans* is investigated in aqueous solutions of increasing viscosity. Detailed flow dynamics associated with the nematode's swimming motion as well as propulsive force and power are obtained using particle tracking and velocimetry methods. We find that *C. elegans* delivers propulsive thrusts on the order of a few nanonewtons. Such findings are supported by values obtained using resistive force theory; the ratio of normal to tangential drag coefficients is estimated to be approximately 1.4. Over the range of solutions investigated here, the flow properties remain largely independent of viscosity. Velocity magnitudes of the flow away from the nematode body decay rapidly within less than a body length and collapse onto a single master curve. Overall, our findings support that *C. elegans* is an attractive living model to study the coupling between small-scale propulsion and low Reynolds number hydrodynamics.
 [doi:10.1063/1.3529236]

I. INTRODUCTION

Considerable progress has been made in the understanding of the motility of swimming micro-organisms at low Reynolds number (Re), which is defined as $\mathrm{Re}=UL/\nu$. Here, U is a characteristic velocity, L is a length scale, and ν is the fluid's kinematic viscosity. For the case of swimming micro-organisms, the length scale is usually small and linear viscous forces typically dominate over nonlinear inertial forces. In the absence of inertia ($\mathrm{Re}\rightarrow 0$), the equations of motion become time-reversible and any net movement attained by the swimmer must result from nonreciprocal motion.[1] Strategies for swimming at low Re include (i) rotation of a helical filament[2,3] and (ii) actuation of a flexible tail to generate propulsive forces.[4–8] The study of this latter mechanism has been motivated in part by early experimental observations of the propulsion of spermatozoa[9] and has been investigated using resistive force theory by Gray and Hancock.[10,11]

In recent years, analytical studies on the motility of micro-organisms at low Re have been complimented by a growing number of experimental investigations. For example, scaled-up models of elastic tails[12,13] and bacterial flagella[14] are commonly used to measure filament shapes, velocity fields, and propulsive forces.[15] At smaller scales, the kinematics of single bacterium have been investigated[16] and the shapes of an oscillating passive actin filament have been probed.[17] Force measurements using optical tweezers have been recently obtained on individual bacteria in an effort to test the validity of resistive force theory[18] and to determine *E. coli* swimming efficiency.

Part of the motivation in studying low Re locomotion lays in the potential impact on technological applications. The development of individual micro- and nanoscale artificial swimmers has rapidly increased, driven by applications such as targeted drug delivery and robotic surgery. One of the leading avenues of such research has been in the use of magnetic fields to actuate artificial bioinspired helical structures in fluids.[19–22] Alternatively, a number of studies have focused on the collective behavior of bacteria swarm, both experimentally[23–27] and theoretically.[23,28–32] Investigations have shown that bacterial suspensions develop transient patterns of coherent locomotion with correlation lengths much larger than the size of individual organisms.[23,26,28] Such collective motion has been used, for example, to induce mixing in microfluidic devices.[25]

Despite recent efforts, there is still a dearth of experimental data on the dynamics of the fluid flows of individual swimming organisms. In particular, there still exist few available measurements of the propulsive force delivered by microswimmers. One limiting reason remains the difficulty in resolving the flows generated by individual micron-scale swimmers such as *E. coli* bacteria or spermatozoa. Perhaps the most well-known flow visualizations of individual undulatory swimming organisms date back to Gray and Lissmann[33,34] nearly half a century ago in which the authors presented qualitative streaklines of freely swimming nematodes in water seeded with starch grains.

In this paper, we characterize the flow behavior of a small undulatory swimmer as function of fluid viscosity by tracking the swimmer's kinematics and by using particle tracking and velocimetry methods. The manuscript is organized as follows. We describe in Sec. II the experimental setup, including the image processing methods and the rheological properties of the aqueous solutions. The organism of choice is the nematode *Caenorhabditis elegans*, a small (~1 mm long), free-living eukaryotic organism widely used

[a)]Present address: Department of Biomedical Engineering, Technion—Israel Institute of Technology, Haifa 32000, Israel.
[b)]Author to whom correspondence should be addressed. Electronic mail: parratia@seas.upenn.edu.

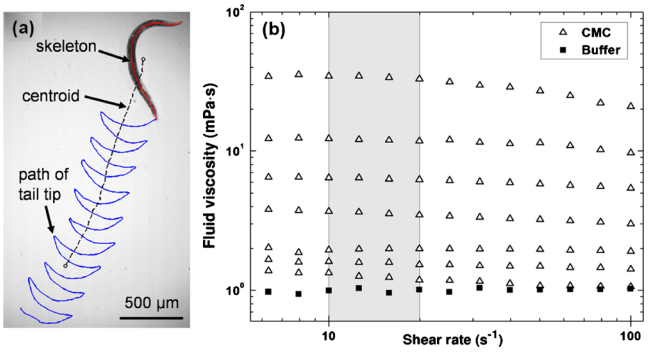

FIG. 1. (Color online) (a) Visualization of the undulatory swimming of *C. elegans*. An instantaneous skeleton (red) of the nematode body is generated by in-house software. The centroid (dashed) and the trajectory of the tail (blue) are tracked at a sampling rate of 125 frames/s. (b) Fluid viscosities (μ) as a function of shear rate for all aqueous solutions. The shear rate ranges from 5 to 100 s^{-1}, and the temperature is maintained at 23 °C. Baseline data (■) correspond to the shear-viscosity of the buffer solution. Triangles (△) represent data for the shear-viscosity of CMC dissolved in buffer solution, at various concentrations by weight. From bottom to top, the concentrations of CMC are respectively 100, 300, 500, 1000, 1500, 2000, and 3000 ppm. The shaded area from 10 to 20 s^{-1} represents the range of measured shear rates in the fluid surrounding the swimming *C.elegans*. Fluid viscosities remain nearly constant within the shaded area; average values in this range are used as the fluid viscosity.

as model system for biological research.[35,36] In Secs. III A–III C the nematode's swimming kinematics are investigated, and estimates of the drag coefficients are presented. In Secs. III D–III F velocity fields are investigated, and estimates of the nematode's (i) propulsive force and (ii) mechanical power are presented. We compare drag coefficient, force, and power estimates from the data to calculations based on resistive force theory. Summary and conclusions follow in Sec. IV. We find that the nematode *C. elegans* is a well-suited organism for low Re swimming investigations. Here, low Re refers to the case in which $\mathrm{Re} < 1$ and inertial forces are negligible. The nematode's periodic swimming behavior allows for high-resolution velocity fields that can be differentiated to estimate propulsive forces and used to characterize low Re flow properties. Kinematic swimming data are coupled with resistive force theory to estimate the ratio of the normal to tangential drag coefficients and compare with analytical values available.

II. EXPERIMENTAL METHODS

A. Experimental setup and fluids

The swimming behavior of *C. elegans* is investigated in small, fluid-filled chambers using a microscope and a high-speed camera as shown in Fig. 1(a). Chambers are made of acrylic and are 1.5 mm wide and 600 μm deep. They are sealed with a thin (0.13 mm) cover glass and are filled with aqueous solutions of varying viscosity. The swimming motion of *C. elegans* is imaged using standard bright-field microscopy (1024×1024 pixels). The depth of focus of the objective (Apochromat 5x/0.16) is 30 μm. The focal plane is set on the longitudinal axis of the nematode body. The nematode beats primarily in the observation plane during the recordings, and the amplitude of the out-of-plane beatings is less than 6% amplitude of planar beatings. All data presented here pertain to nematodes swimming at the center of the fluidic chamber. Out-of-plane recordings are discarded. The spatial resolution is approximately 4.00 μm/pixel. The image acquisition rate is kept constant at 125 frames/s (fps) in order to resolve small linear displacements along the nematode's body between consecutive frames. Wild type (N2) strains of *C. elegans* are obtained from the *Caenorhabditis elegans* Genetic Stock Center (University of Minnesota). Adult nematodes are maintained on agar plates using standard culture methods[35] and fed with bacteria *E. coli* strain OP50.

TABLE I. Polymer concentration and corresponding shear-viscosities of all solutions investigated. The 0 ppm case corresponds to the buffer solution.

CMC concentration (ppm)	Solution viscosity (mPa s)
0	1.0
100	1.3
300	1.6
500	2.0
1000	3.6
1500	6.3
2000	12.0
3000	34.5

Fluids of different viscosities (μ) are prepared by adding small amounts of carboxymethyl cellulose (CMC) ($\mathrm{MW} = 2.1 \times 10^6$) to a M9 buffer solution.[35] The concentration of CMC in buffer solution ranged from 100 to 3000 ppm. The solutions' shear-viscosities range from 1.0 mPa s (buffer solution) to 34.5 mPa s, as shown in Table I. The polymer CMC has a flexible backbone such that viscoelastic effects are expected to arise in the fluids.[37] However, the salt ions in the buffer solution screen the polymer molecules. This screening tends to keep the molecule in the coiled state even at moderate strain-rates (≈ 10 s^{-1}). As a result, viscoelastic and strain-rate dependent viscosity behaviors are minimized. Figure 1(b) shows the fluid shear-viscosity versus shear-rate for all solutions. Note that the shear-viscosities are nearly constant even for the highest concentration solutions investigated here. No appreciable first normal stress-difference (N1) is observed for all solutions.

B. Nematode tracking: Kinematics

The nematode kinematics are characterized using in-house image analysis codes.[38] In short, for each instantaneous snapshot of the swimming nematode, segmentation is used to extract the nematode's body shapes and centroid positions. We track uniformly distributed points along the nematode's body centerline (i.e., *skeleton*), which is described by a continuous, differentiable two-dimensional (2D) spline curve. Note that *C. elegans* does not possess an actual skeleton, and the nomenclature used here refers to topological skeletons. For this step, a morphological segmentation[39]

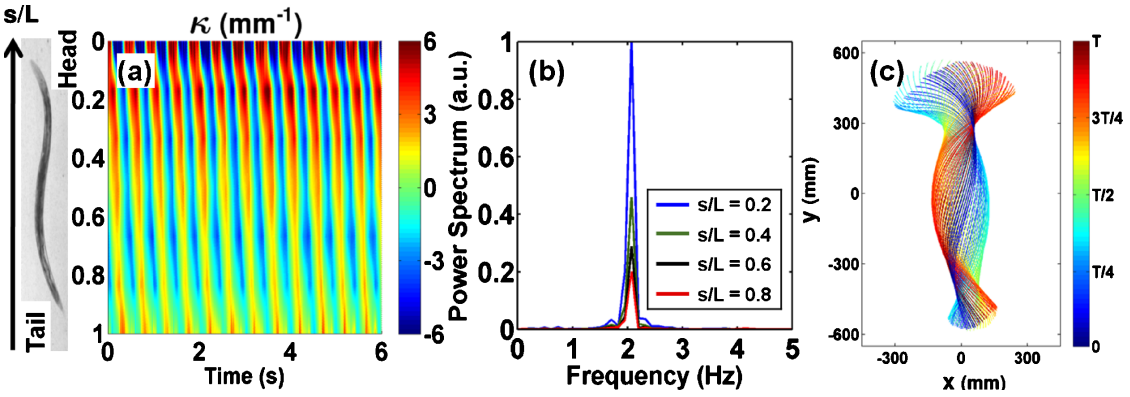

FIG. 2. (Color online) The kinematics of swimming *C. elegans* at low Re in a viscous M9 buffer solution. (a) Contour plot of the measured curvature (κ) along the nematode's skeleton as a function of time. The y-axis corresponds to the dimensionless position s/L along the nematode's body, where $s=0$ is the head and $s=L$ the tail. (b) Frequency spectra of κ at different selected positions s/L. The nematode's beating frequency peaks at a single value (~2.0 Hz), irrespective of the location s/L. (c) Temporal evolution of nematode skeletons over one beating cycle of period T (~0.5 s). The nematode is aligned vertically upward along the y-axis; note that the nematode head manifests the largest beating amplitude.

is performed on the nematode's binary images. This procedure removes pixels on the boundaries of the object but does not allow the object to break apart such that the pixels remaining make up an image skeleton. Next, a corner-detection algorithm[40] is used to identify the x-y coordinates of the head and tail. Finally, in order to build smooth 2D curves, an algorithm is developed to sample the nematode's skeleton using a sequential Monte Carlo Markov chain approximation.[41] Hence, skeletons approximate the nematode's body posture at any given instant in time [Fig. 1(a)] and the nematode swimming speed (U) can be calculated by differentiating the nematode centroid position with respect to time.

The nematode's swimming behavior is further characterized by measuring the bending curvature $\kappa(s,t)$ along the nematode's body centerline.[38] The curvature is defined as $\kappa(s,t)=d\phi/ds$. Here, ϕ is the angle made by the tangent to the x-axis in the laboratory frame at each point along the body centerline and s is the arc length coordinate spanning the head of the nematode ($s=0$) to its tail ($s=L$). The largest bending amplitude A is computed at the nematode's head.

C. Particle tracking: Velocity fields

Fluid velocity fields generated by swimming nematodes are obtained using both particle tracking[42] and image velocimetry methods.[43] For both methods, the fluid is seeded with 2.2 μm green fluorescent polymer microspheres (Duke Scientific Corp., CA). The seeding particles show negligible Brownian motion compared to the flow velocity ($V\approx 0.5$ mm/s). The Péclet number, defined as $\mathrm{Pe}=VL/D$, is on the order of $O(10^6)$, where D is the diffusion coefficient of the aqueous solution. In particle tracking, the seeding particles are tracked continuously for the entire duration of the experiment. Velocities are computed from the local particle displacements. In particle image velocimetry (PIV), the instantaneous velocity field is obtained using cross-correlation methods with a window size of 16 by 16 pixels. Both tracking and PIV methods produce similar velocity fields.

III. RESULTS AND DISCUSSION

A. Nematode kinematics

Nematodes are typically tracked over multiple bending cycles using image analysis. In Fig. 1(a), a representative *C. elegans* tracked over approximately 10 cycles in the pure buffer solution ($\mu=1.0$ mPa s) is shown. We find that nematodes swim with an average speed (U) of 0.36 ± 0.01 mm/s. Nematodes also display a characteristic periodic beating pattern as illustrated by the trajectories swept by the *C. elegans*' tail [Fig. 1(a)]. For such swimming behavior, the Re is approximately 0.38, based on the nematode's body length L (1.06 ± 0.06 mm) and swimming speed U.

A contour plot of the spatiotemporal evolution of the curvature $\kappa(s,t)$ for a *C. elegans* swimming in buffer solution ($\mu=1.0$ mPa s) is shown in Fig. 2(a) for approximately ten beating (or swimming) cycles. The curvature values are color-coded, such that red and blue represent positive and negative values of κ, respectively. In Fig. 2(a), the x-axis corresponds to time, while y-axis corresponds to the nondimensional position s/L along the length of the nematode's body. The contour plot reveals the existence of periodic and well-defined diagonally oriented lines. These diagonal lines are characteristics of bending waves which propagate from head to tail. Such waves are known to correspond to the alternating phases of dorsal and ventral contractions driven by rhythmic activity of the 95 muscle cells that line the nematode's body.[44,45]

The nematode's body bending frequency f is obtained by computing the one-dimensional fast Fourier transform of the spatiotemporal curvature field $\kappa(s,t)$ at multiple body positions s/L, as shown in Fig. 2(b).[38] A single frequency peak in the Fourier spectrum is found at $f\approx 2.0$ Hz for the nematode shown in Fig. 1(a). This frequency is nearly independent of body position s/L. This follows as the contour plot of curvature [Fig. 2(a)] shows a single traveling wave propagating in which the magnitude of the body curvature decreases from head to the tail along the nematode body; the entire nema-

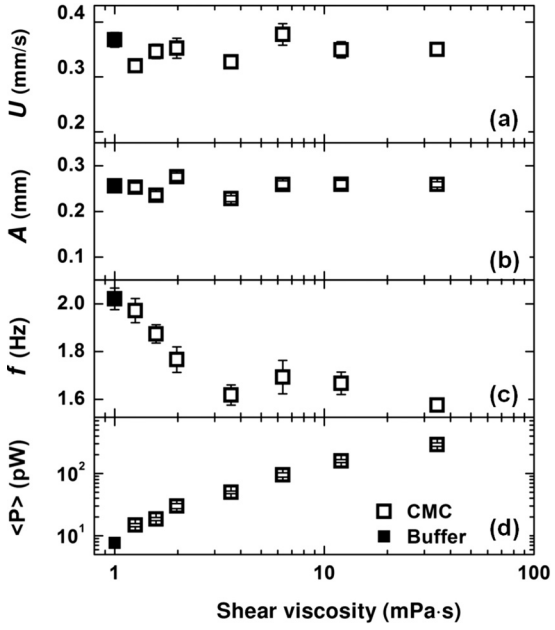

FIG. 3. Effects of fluid viscosity (μ) on the kinematics of swimming *C. elegans*. Measurements for three kinematic metrics are shown. (a) Mean forward swimming speed (U). (b) The beating amplitude (A). (c) Body bending frequency (f). (d) Mean propulsive power ($\langle P \rangle$). The data are obtained by tracking 10~20 nematodes at varied shear-viscosities in the buffer and CMC solutions. The fluid viscosity ranges from 1.0 to 34.5 mPa s. The swimming speed and beating amplitude remain constant within the viscosity range while the beating frequency exhibits a 20% decay as the fluid viscosity increases.

tode population tested here swims at nearly the same frequency, with very little spread in the data (see Fig. 3).

Figure 2(c) illustrates the color-coded temporal evolution of nematode centerlines (or skeletons) over one representative beating cycle of period $T=0.5$ s; the nematode is oriented with its head vertically upward. Recently, it has been shown that such body postures may be described analytically by a superposition of traveling waves.[38] We note that the nematode beating pattern is reasonably symmetrical along the length of its body, but the swimming gait is asymmetric in the sense that the largest beating amplitudes are observed at the head.[38] This asymmetry is perhaps a feature characteristic undulatory swimmers of finite body length, and it may be required for net forward propulsion at low Re.[1]

B. Nematode motility: Fluid viscosity effects

Motility metrics including nematode's swimming speed (U), amplitude (A), and beating frequency (f) are shown as a function of fluid viscosity in Figs. 3(a)–3(c), respectively. While the fluid viscosity yields more than a tenfold increase in the effective mechanical load on swimming *C. elegans*, we note that the nematode swimming speed (U) remains constant at approximately 0.35 mm/s over the viscosity range [Fig. 3(a)]; such viscosity-independent results are in accordance with Taylor's predictions for swimming speeds of an undulating sheet at Re=0.[6]

The nematode beating amplitudes remain constant at approximately 0.25 mm [Fig. 3(b)] and is independent of fluid viscosity. Concurrently, wild-type *C. elegans* are able to modulate their beating frequency [Fig. 3(c)]; we note a decrease in the magnitude of the nematode beating frequency (f) from 2.0 to 1.6 Hz over the viscosity range. Such findings are supported by previous work demonstrating *C. elegans* ability to adapt its motility behavior to different fluidic solutions.[37,45,46] It is interesting to mention that if the beating frequency decreases [Fig. 3(c)] and the amplitude remains constant [Fig. 3(b)], one would expect the swimming speed (U) to decrease for increasing fluid viscosity. However, the validity of such statement is mainly based on the assumption that *C. elegans* is power-limited and thus unable to sustain a constant swimming speed. In contrast, we find that the mean power ($\langle P \rangle$) of swimming nematodes increases with fluid viscosity [Fig. 3(d)]; details on the computation of $\langle P \rangle$ are provided in Sec. III F. Such results are also supported by a previous experimental investigation where mechanosensory input affects the temporal frequency of the nematode's swimming gait.[46] Despite the nematodes' ability to adapt to the fluidic environment, it still remains unclear why the temporal gait is modulated, and how does it not simultaneously affect the spatial form of the swimming gait.[38,45,46]

C. Nematode kinematics: Swimming speed and drag coefficients

In this section, the nematode's swimming speed is compared to predictions obtained using resistive force theory.[10,11,47,48] We note that the ratio between the nematode's length ($L=1$ mm) and diameter ($d=80$ μm) is approximately $L/d \sim 12$. Hence, in the limit of low Re, nematodes can be treated as slender bodies moving in viscous fluids where inertial effects are negligible. Under such conditions, the net thrust of propulsive force (F_{prop}) produced by an undulating filament is balanced by the drag force (F_{drag}) imposed from the surrounding fluid, such that $F_{\text{prop}}+F_{\text{drag}}=0$. An expression for the swimming speed (U) of an undulating filament was proposed by Gray and Hancock,[11] and is given by

$$U = 2\pi^2 f \lambda \frac{\left(\frac{A}{\lambda}\right)^2 \left(\frac{C_N}{C_T} - 1\right)}{1 + 2\pi^2 \left(\frac{C_N}{C_T}\right)\left(\frac{A}{\lambda}\right)^2}, \quad (1)$$

for the case of large amplitude displacements. In Eq. (1), λ is the filament wavelength, A is the constant body amplitude, which is independent of position along the body length, and f is the beating frequency. The variables C_N and C_T are the normal and tangential drag coefficients, respectively. For the case of *C. elegans* swimming in buffer solution (1.0 mPa s), the experimental values of λ, A, and f are 1 mm, 0.25 mm, and 2.02 Hz, respectively. The swimming speed U is 0.36 mm/s.

An estimate of the drag coefficient ratio C_N/C_T can be obtained by using the experimental data and Eq. (1). We find that, for a nematode swimming in a waterlike, Newtonian

TABLE II. Drag coefficient ratio (C_n/C_t) and corresponding swimming speed obtained using Eq. (1) as estimated from experiments and analytical values from previous studies.

	C_N/C_T	U (mm/s)
Experiments	1.4	0.36
Gray and Lissmann[a]	1.4–1.6	0.36–0.50
Lighthill[b]	1.5	0.43
Gray and Hancock[c]	2.0	0.7
Katz *et al.*[d]	4.1	1.4

[a]Reference 34.
[b]Reference 48.
[c]Reference 9.
[d]Reference 47.

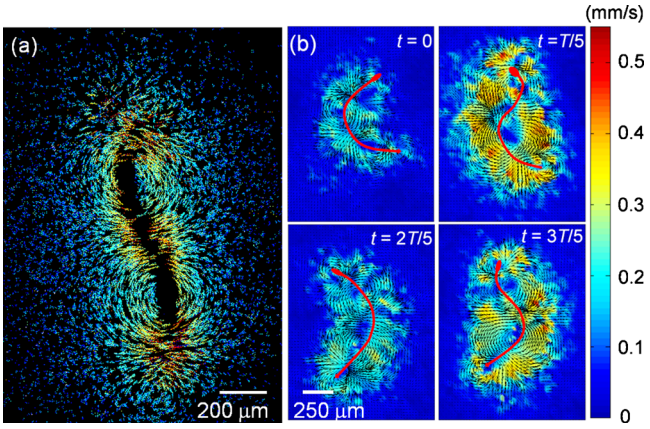

FIG. 4. (Color online) Velocity fields and flow behavior a swimming *C.elegans*. The nematode shown is tracked in the buffer solution. (a) Color/shade-coded particle pathlines are shown via the trace of dispersed fluorescent particles. Particle trajectories are tracked over ten consecutive frames (~0.06 s). Colors/shades are associated with the lengths of trajectories. Two dominant recirculation regions are resolved along the nematode body. (b) PIV flow fields of the fluid surrounding a swimming *C.elegans* at $t=0$, $T/5$, $2T/5$, and $3T/5$. The vectors indicate the directions of the fluid velocity at each points and the color field illustrates the magnitude of the flow (in mm/s).

fluid C_N/C_T is approximately 1.4. This value is very similar to the ones reported by Gray and Lissmann,[34] who dropped thin wires into viscous fluids and estimated swimming speeds ranging from 0.36 to 0.50 mm/s using Eq. (1). By comparison, Lighthill[48] obtained $C_N/C_T=1.5$ for the case of an undulating filament swimming in an infinite fluid medium at low Re. The estimated swimming speed for $C_N/C_T=1.5$ using Eq. (1) is 0.43 mm/s. A larger value of the ratio of drag coefficients ($C_N/C_T=4.1$) is obtained using the corrections of Katz *et al.*[47] who incorporated wall-effects into their analysis. Correspondingly, the estimated swimming speed is 1.4 mm/s. By using resistive force theory, which does not consider hydrodynamic interactions, Gray and Hancock[9] showed that the value of C_N/C_T is equal to 2; the estimated swimming speed using Eq. (1) is 0.7 mm/s. Results are summarized in Table II.

Overall, the analytical values of the ratio C_N/C_T provide reasonably good estimates for the swimming speed of a finite undulating slender body, such as *C. elegans*, moving in a viscous fluid. The analysis proposed by Lighthill,[48] in which hydrodynamic interactions are considered, provides good estimates for the swimming speed (or drag coefficients). The estimated swimming speed is 0.43 mm/s which is higher than the experimental value of 0.35 mm/s. A possible source of error may be confinement effects. However, the relatively small values of the drag coefficient ratio obtained using experimental data ($C_N/C_T=1.4$) suggest that confinement effects may not be important. We note that for fixed waveforms, an increase in inertial effects (i.e., Re increases) for an undulating sheet in a viscous fluid will lead to a decrease in its resulting self-propulsive speed;[49] such analytical prediction may help understand the difference observed between the theoretical speed, where Eq. (1) is valid at Re=0, and the smaller measured speeds, which correspond to a departure from Re=0.

D. Velocity fields

The fluid flow behavior of swimming nematodes is investigated using particle tracking and velocimetry methods. An example of particles trajectories over one beating cycle for a nematode swimming in buffer solution is shown in Fig. 4(a). The trajectories are color-coded such that red and blue correspond to long and short displacements, respectively. Long particle displacements and recirculating trajectories are observed near the nematode's body. Such patterns are similar to the qualitative visualizations of Gray and Lissmann,[34] who associated the circulation of particles around a nematode's body with regions of maximum transverse body displacement.

Figure 4(b) shows instantaneous, two-dimensional velocity fields for a nematode swimming in buffer solution. Velocity fields are presented at equal time intervals ($\Delta t=0.1$ s) over a representative body bending cycle. A common feature of the flow field over time is the regions of fluid recirculation that are aligned along the nematode's body. These recirculation regions persist throughout the bending cycle, but their exact location varies. In general, three to four recirculation regions are observed along the nematode's body for fluid viscosities ranging from 1.0 to 34.5 mPa s. Recirculating flow structures, or vortices, exhibits a typical length scale on the order of $L/4$ to $L/3$, and pairs of adjacent vortices are seen to rotate in opposite directions. The vortices generated by *C. elegans* swimming remain attached within the vicinity of the nematode's body rather than being shed off into the fluid, which is a hallmark of low Re flows.

Next, the temporal properties of the velocity fields are investigated as a function of fluid viscosity. Figure 5 (left column) shows the spatially averaged velocity magnitude $\langle|V|\rangle$ as a function of time and the corresponding normalized power spectra $P(f)$ (right column). The fluid viscosities are 1.0 mPa s [Figs. 5(a) and 5(b)], 3.6 mPa s [Figs. 5(c) and 5(d)], 12.0 mPa s [Figs. 5(e) and 5(f)], and 34.5 mPa s [Figs. 5(g) and 5(h)], respectively. The quantity $\langle|V|\rangle$ is computed by defining a region of interest in the flow where velocities are larger than 10% of the maximum velocity magnitude in each instantaneous velocity field. This region spans

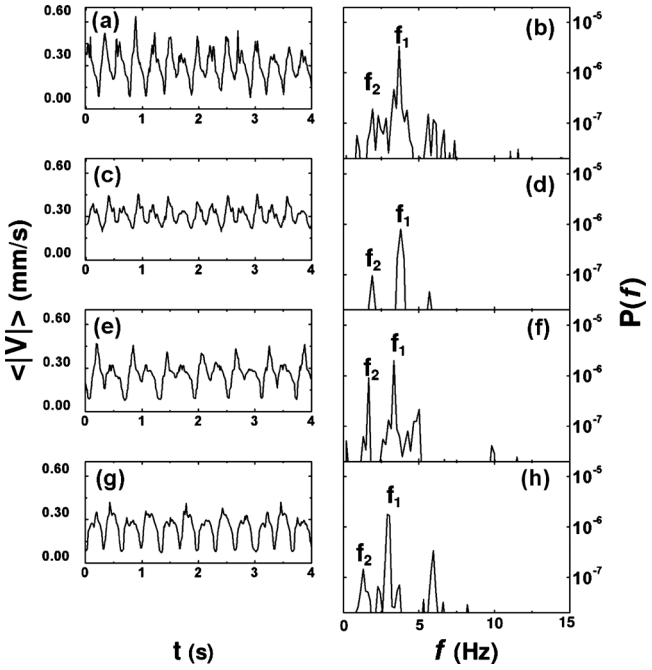

FIG. 5. Temporal signals of the mean fluid velocity magnitude $\langle|V|\rangle$ (left column) and corresponding normalized power spectrum (right column) in buffer and CMC solutions of varying viscosity. Fluid viscosities are [(a) and (b)] μ=1.00 mPa s (M9), [(c) and (d)] μ=3.60 mPa s (1000 ppm CMC), [(e) and (f)] μ=12.0 mPa s (2000 ppm CMC), and [(g) and (h)] μ=34.5 mPa s (3000 ppm CMC). Power spectrum is normalized by the mean squared amplitude. Temporal signals of $\langle|V|\rangle$ are characterized by double-peaks of varying magnitudes (left column). The alternating peaks in $\langle|V|\rangle$ are manifested as two dominant frequency peaks (f_1 and f_2) in the power spectrum (right column). The ratio of f_1 to f_2 remains approximately 1/2 for all four solutions; f_1 is observed to be the nematode beating frequency, while f_2 is associated with the alternating dorsal and ventral beating motions in one beating cycle. The slight shift in frequency peaks to the left indicates the decreasing beating frequency in fluids of higher viscosities, as seen in the kinematic data [Fig. 4(c)].

approximately one body length (1 mm) in all directions. This is done so that the statistics are not biased by the presence of nearby zero values away from the nematode. The quantity $\langle|V|\rangle$ is the spatially averaged velocity magnitude in that particular region of interest. Results show that $\langle|V|\rangle$ possesses a periodic behavior in time with a characteristic double period. The periodic fluid behavior is a response to the nematode's periodic beating pattern, which is attenuated as the fluid viscosity is increased.

The power spectra of the velocity signal are shown in Fig. 5 (right column). The data show that, for the range of viscosities investigated, there exist two characteristic frequencies f_1 and f_2. Here, f_1 is the dominant frequency and is approximately twice f_2 for all four fluids. The velocity signal resurges twice in each period because the nematode beats alternately on its dorsal and ventral sides throughout one beating cycle. In the power spectra, the nematode undulating frequency is shown as the peak f_2, and the bilateral beating gaits in each cycle are captured by the peak $f_1 \approx 2f_2$. Beyond 5 Hz, all discernible peaks suggest harmonic echoes of the two primary frequencies in addition to small noise associated with the measurements.

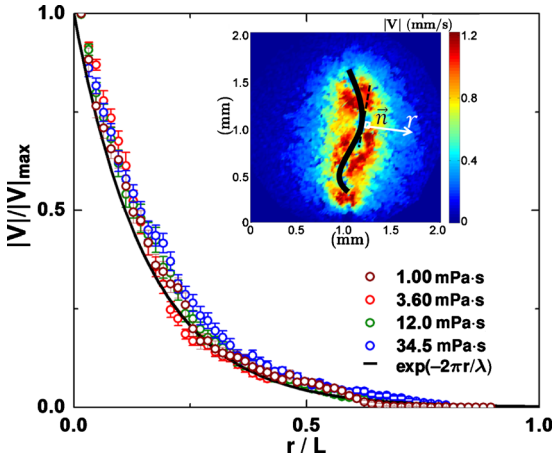

FIG. 6. (Color online) Normalized fluid velocity magnitude ($|V|/|V|_{max}$) as a function of the nondimensional distance (r/L) away from the nematode body, where r=0 represents the boundary of the nematode body and L is the nematode body length. The plots of different colors/shades correspond to fluids of different viscosities. Each data point corresponds to the ensemble average value computed for various locations along the nematode body and instances in time over one beating cycle. The solid line corresponds to the expression $\exp(-2\pi r/\lambda)$ (Ref. 48). Inset: representative velocity magnitude field ($|V|$) at a given instant in time in the buffer solution. The local normal vector along the nematode body is depicted as $\vec{n}$ and the distance r increases along the direction of $\vec{n}$.

E. Velocity fields: Are *C. elegans* low Re swimmers?

In this section, the flows generated by the nematodes are used to address whether the nematode *C. elegans* can be considered a low Reynolds number swimmer. For the experiments performed here, the Re based on the nematode's length and swimming speed ranges from 0.4 to 0.01 as the fluid viscosity is increased from 1 to 34.5 mPa s. The fluid flow of low Re swimmers is governed by linear viscous forces. Hence, the form of the velocity decay normal to the swimming nematode should be independent of viscosity.

In Fig. 6, the velocity magnitude of the fluid ($|V|$) is shown as a function of the normalized distance (r/L) away from the nematode body for fluids of different viscosities. Here, the velocity is normalized with respect to its maximum value ($|V|_{max}$). Curves are obtained from ensemble averages over eight cross-sectional locations uniformly distributed along the nematode body and five instantaneous time points within a representative body bending cycle, i.e., t=0, $T/4$, $T/2$, $3T/4$, and T. The distance r away from the nematode is measured in the normal direction away from the body boundary, as schematically illustrated in the inset of Fig. 6. Once normalized, the velocity decay profiles collapse onto a single master curve. Beyond one body length (L) away from the nematode, the fluid flow is quiescent. This collapse indicates that the flows in the vicinity of the nematodes are largely similar with Re from 0.4 to 0.01. Hence, one can safely consider *C. elegans* to be a low Re swimmer for the viscosity range investigated here. We note that the normalized velocity decay follows closely an exponential decay of the form $\sim\exp(-2\pi r/\lambda)$ obtained by Lighthill[48] for an undulating sheet in Stokes flow (i.e., Re=0), where λ is the characteristic wavelength and r is the distance from the swimming body.

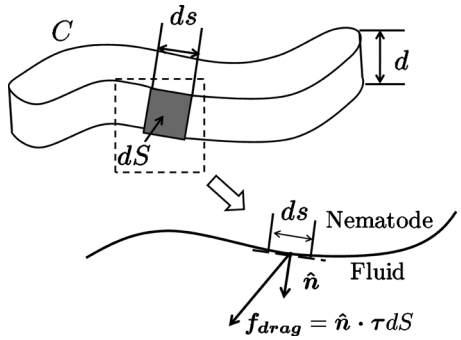

FIG. 7. Schematic illustration of the modeled nematode body shape for force and power calculation. The nematode body is assumed to be an extruded volume of thickness d bounded by the shape contour C. The shaded area segment (dS) represents a infinitesimal rectangular element on the lateral side of the body of length ds. $\hat{n}$ is the unit normal vector of the area segment pointing away into the fluid. The local fluid stress on dS is given by $\hat{n}\cdot\tau$. The local drag acting upon dS by the fluid follows as $f_{\text{drag}}=\hat{n}\cdot\tau dS$.

F. Velocity fields: Propulsive force and power

The propulsive force generated by the nematode *C. elegans* swimming at low Reynolds number is calculated using the fluid velocity fields and nematode body postures. The velocity fields are differentiated in space and time to obtain velocity gradients and the corresponding strain-rate field. The fluid shear-stress is then calculated using the known values of the fluid viscosity [see Fig. 1(b) and Table I]. The drag force on the nematode body is calculated by integrating the shear-stress over the nematode body surface. In the limit of low Re, the total force on the swimming nematode is zero and the nematode propulsive force is balanced by the fluid drag force, such that $F_{\text{prop}}(t)+F_{\text{drag}}(t)=0$.

The hydrodynamic drag force F_{drag} on the swimming nematode is calculated on a body of thickness d that is bounded by a shape contour C (Fig. 7). The body's thickness is 80 μm, corresponding to the nematode diameter, and the shape contour is experimentally obtained using image analysis. The drag force on each area segment dS (Fig. 7) is given by $f_{\text{drag}}=\hat{n}\cdot\tau dS=\hat{n}\cdot\tau(ds\cdot d)$, where $\hat{n}$ is the unit normal vector and τ is the fluid stress defined as $\tau=\mu\dot{\gamma}=\mu(\nabla\vec{V}+\nabla\vec{V}^T)$. Here, $\dot{\gamma}$ is the shear-rate. Hence, the local fluid stress and the local drag force on each segment can be obtained. The total drag force is computed by integrating over the entire body surface, such that $F_{\text{drag}}(t)=\int_C f_{\text{drag}}=\int_C ds\cdot\hat{n}\cdot\tau\cdot d$. Using the overall force balance, the propulsive force is then $F_{\text{prop}}(t)=-F_{\text{drag}}=-\int_C ds\cdot\hat{n}\cdot\tau\cdot d$. The corresponding mechanical power is $P(t)=-\int_C f_{\text{drag}}\cdot\vec{V}$. Thus, the total propulsive force and mechanical power can be obtained at each instant over a swimming cycle. Here, the power dissipated in viscous shear (P) represents a lower limit on the total power that the nematode uses to swim.[45] In addition, one should note that estimates of F_{prop} and P include only the contributions of fluid stresses on the sides of the model body shape (Fig. 7) but neglect the additional contributions from top and bottom surfaces, where velocimetry data are unavailable. Hence, our approximation should be interpreted as an underestimate of the total propulsive force and power delivered in reality by nematodes.

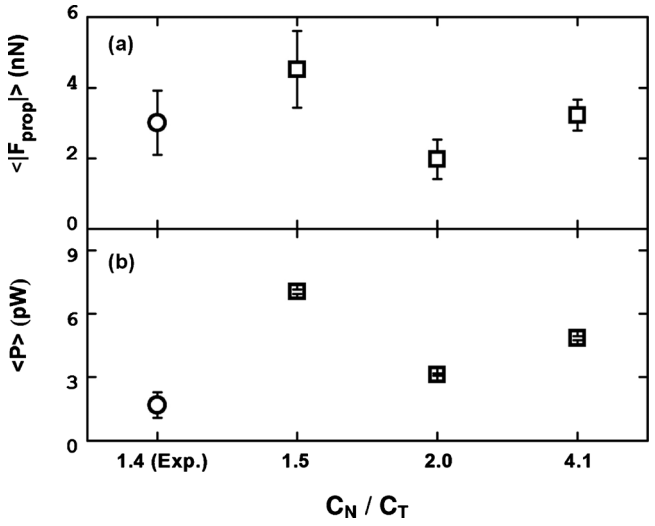

FIG. 8. Magnitudes of the propulsive forces ($\langle|F_{\text{prop}}|\rangle$) and corresponding powers ($\langle|P|\rangle$) averaged over one beating period. Data are down as (a) calculated using experimental velocimetry and rheological data (exp.), which corresponds to an estimated value of $C_n/C_t=1.4$ [Eq. (1)], and (b) as obtained from previous studies (Table II). Error bars show the standard deviations of the average values.

The magnitude of the propulsive force $\langle|F_{\text{prop}}|\rangle$ and the mechanical power $\langle P\rangle$ averaged over one swimming cycle is shown in Fig. 8. The error bars are the standard deviations of the averages. The calculated experimental values for the force and power are 3.0 nN and 1.7 pW, respectively. The values of propulsive force and power computed using the experiments (Fig. 8) are similar to those obtained using analytical predicted values of the ratio of normal to tangential drag coefficient C_N/C_T,[11,47,48] as discussed in Sec. III C. One should note that analytical values of the propulsive force and power, where $\langle P\rangle=(1/T)\int_0^T\int_0^L C_N u_N(s,t)^2+C_T u_T(s,t)^2 dsdt$ (this expression is also used to compute the data of Fig. 3(d), where C_N and C_T are obtained from Katz *et al.*[11,47,48]), still require the use of kinematic data for the velocity distribution along the nematode body (i.e., normal u_n and tangential u_t velocities). That is, the experimental data obtained here are used in conjunction with theoretical values of C_N and C_T to compute the so-called analytical values of $\langle|F_{\text{prop}}|\rangle$ and $\langle P\rangle$. In contrast, experimental values of $\langle|F_{\text{prop}}|\rangle$ and $\langle P\rangle$ rely on velocimetry data only, as obtained from PIV measurements. The ratio $C_N/C_T=1.4$ is shown in Fig. 8 for clarity, relative to analytical predictions of the ratio $C_N/C_T=1.5$, 2.0, and 4.1. To our knowledge, these measurements are among the first estimations of propulsive force and power performed for low Re swimmers.

In order to gain further insight into the nematode's swimming mechanism, the propulsive force is decomposed into a tangential force (thrust) F_T and a normal force (lateral force) F_N, as shown in Fig. 9. The tangential force is the component of the propulsive force along the swimming direction, and the normal force is the component of the propulsive force in the direction perpendicular to the swimming direction. The normalized profile of the tangential and normal components of the propulsive force as a function of a swimming cycle is shown in Fig. 9. The force components

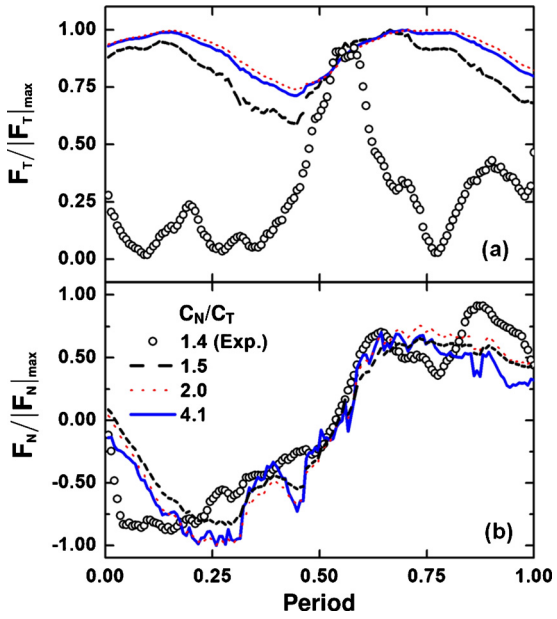

FIG. 9. (Color online) Normalized tangential ($F_T/|F_T|_{max}$) and normal forces ($F_N/|F_N|_{max}$) over one swimming cycle. Circles (○) represent the experimental measurement results, which corresponds to an estimated drag coefficient ratio $C_n/C_t=1.4$. The estimated normalized (a) tangential and (b) normal forces are also computed according to analytical values of the drag coefficient ratio (Table II). The experimentally measured normalized tangential force exhibits an impulsive pattern that differs from the patterns seen in the other three results. All four normalized normal forces share a similar profile. The relative error of the experimental force measurement data is 11%, 8% of which is contributed by the small deviations of the nematode swimming gaits between periods.

are normalized with respect to their maximum absolute values. The time signal of the experimentally determined tangential force exhibits an impulselike peak in the middle of the swimming cycle, which spans for approximately 1/4 period. This impulse is responsible for most of the swimming momentum. At the time when the tangential force reaches its peak value, the normal force vanishes. The experimental force profiles are compared to estimates using the aforementioned models (Fig. 9). The experimental and analytical profiles of the normal component are very similar; in the first half of a period, the nematode produces a negative normal force while in the second half, the nematode produces a net positive force after having flipped onto its other side. On the other hand, the analytical tangential profiles display a sustained thrust while the experiments show a clear impulse. The force decomposition data suggest that the nematode swims forward via a series of periodic impulses that are generated in the middle of beating cycles.

IV. SUMMARY AND CONCLUSIONS

In this paper, we present an experimental investigation of undulatory swimming phenomena for the nematode *C. elegans*. Here, nematodes are observed swimming in aqueous solutions of increasing viscosity (1–34.5 mPa s). Using kinematic data for nematode locomotion such as swimming speed (U), beating amplitude (A), and frequency (f), we estimate the ratio of normal to tangential drag coefficients (C_N/C_T) using resistive force theory; our experimental value of $C_N/C_T=1.4$ compares well with analytical predictions from previous studies (Table II). Conversely, we find that analytical values of C_N/C_T provide reasonably accurate predictions of the nematode swimming speed. To the best of our knowledge, we provide the first noninvasive estimations of propulsive force and power delivered by *C. elegans* based solely on flow velocimetry data. We find that experimental values are close to estimates using resistive force theory (Fig. 8). In addition, the magnitudes of our measured forces are supported by recent experimental measurements of force delivered by crawling *C. elegans* using force-sensing micropillars,[50] with $\langle F_{prop}\rangle \sim 2$ nN.

By investigating the dynamics of fluid flow, we have attempted to answer the question whether the nematode *C. elegans* is a low Reynolds number swimmer. First, we find that the nematode's characteristic Reynolds number, based on body length and swimming speed, ranges between Re =0.4 and 0.01 as the fluid viscosity is increased; such values always remain below unity. Our velocimetry data exhibit hallmarks of low Reynolds number flows. Namely, the dynamics of the flow are overwhelmingly independent of the fluid viscosity. This is shown at all viscosities investigated in (i) the recirculating flow structures which remain attached along the swimming nematode (Fig. 4) as well as in (ii) the frequency responses of the flow which display a characteristic double period signature across (Fig. 5). Finally, normalized velocity profiles of the flow away from the nematode collapse onto a single master curve (Fig. 6). Such rapid velocity decay away from the body follows closely the exponential form predicted for an undulating sheet subject to Stokes flow conditions.[48] Altogether, our results suggest that the nematode *C. elegans* provides an attractive model to study low Reynolds number locomotion. Such living organism offers an ideal candidate to bridge our understanding of low Reynolds number hydrodynamics with small-scale propulsion.

ACKNOWLEDGMENTS

The authors gratefully acknowledge P. Krajacic and T. Lamitina for their assistance with *C. elegans,* and P. K. Purohit and A. J. Smits for fruitful discussions. Special thanks to P. Rockett for manufacturing the acrylic channels. This work was supported by NSF CAREER Award No. CBET-0954084.

[1] E. M. Purcell, "Life at low Reynolds-number," Am. J. Phys. **45**, 3 (1977).
[2] E. M. Purcell, "The efficiency of propulsion by a rotating flagellum," Proc. Natl. Acad. Sci. U.S.A. **94**, 11307 (1997).
[3] N. Coq, O. du Roure, M. Fermigier, and D. Bartolo, "Helical beating of an actuated elastic filament," J. Phys.: Condens. Matter **21**, 204109 (2009).
[4] J. M. Lighthill, *Mathematical Biofluiddynamics* (Society for Industrial Mathematics, Philadelphia, 1987).
[5] K. E. Machin, "Wave propagation along flagella," J. Exp. Biol. **35**, 796 (1958).
[6] G. Taylor, "The action of waving cylindrical tails in propelling microscopic organisms," Proc. R. Soc. London, Ser. A **211**, 225 (1952).
[7] E. Lauga, "Floppy swimming: Viscous locomotion of actuated elastica," Phys. Rev. E **75**, 041916 (2007).
[8] C. H. Wiggins and R. E. Goldstein, "Flexive and propulsive dynamics of elastica at low Reynolds number," Phys. Rev. Lett. **80**, 3879 (1998).
[9] J. Gray, "The movement of sea-urchin spermatozoa," J. Exp. Biol. **32**, 775 (1955).

[10]C. Brennen and H. Winet, "Fluid-mechanics of propulsion by cilia and flagella," Annu. Rev. Fluid Mech. **9**, 339 (1977).
[11]J. Gray and G. J. Hancock, "The propulsion of sea-urchin spermatozoa," J. Exp. Biol. **32**, 802 (1955).
[12]B. Qian, T. R. Powers, and K. S. Breuer, "Shape transition and propulsive force of an elastic rod rotating in a viscous fluid," Phys. Rev. Lett. **100**, 078101 (2008).
[13]T. S. Yu, E. Lauga, and A. E. Hosoi, "Experimental investigations of elastic tail propulsion at low Reynolds number," Phys. Fluids **18**, 091701 (2006).
[14]M. Kim, J. C. Bird, A. J. van Parys, K. S. Breuer, and T. R. Powers, "A macroscopic scale model of bacterial flagellar bundling," Proc. Natl. Acad. Sci. U.S.A. **100**, 15481 (2003).
[15]M. J. Kim, M. J. Kim, J. C. Bird, T. R. Powers, and K. S. Breuer, "Particle image velocimetry experiments on a macro-scale model for bacterial flagellar bundling," Exp. Fluids **37**, 782 (2004).
[16]J. Yang, C. W. Wolgemuth, and G. Huber, "Kinematics of the swimming of spiroplasma," Phys. Rev. Lett. **102**, 218102 (2009).
[17]C. H. Wiggins, D. Riveline, A. Ott, and R. E. Goldstein, "Trapping and wiggling: Elastohydrodynamics of driven microfilaments," Biophys. J. **74**, 1043 (1998).
[18]S. Chattopadhyay and X. L. Wu, "The effect of long-range hydrodynamic interaction on the swimming of a single bacterium," Biophys. J. **96**, 2023 (2009).
[19]R. Dreyfus, J. Baudry, M. L. Roper, M. Fermigier, H. A. Stone, and J. Bibette, "Microscopic artificial swimmers," Nature (London) **437**, 862 (2005).
[20]P. Garstecki, P. Tierno, D. B. Weibel, F. Saguès, and G. M. Whitesides, "Propulsion of flexible polymer structures in a rotating magnetic field," J. Phys.: Condens. Matter **21**, 204110 (2009).
[21]A. Ghosh and P. Fischer, "Controlled propulsion of artificial magnetic nanostructured propellers," Nano Lett. **9**, 2243 (2009).
[22]L. Zhang, J. J. Abbott, L. Dong, K. E. Peyer, B. E. Kratchovil, H. Zhang, C. Bergeles, and B. J. Nelson, "Characterizing the swimming properties of artificial bacterial flagella," Nano Lett. **9**, 3663 (2009).
[23]L. H. Cisneros, R. Cortez, C. Dombrowski, R. E. Goldstein, and J. O. Kessler, "Fluid dynamics of self-propelled microorganisms, from individuals to concentrated populations," Exp. Fluids **43**, 737 (2007).
[24]M. J. Kim and K. S. Breuer, "Controlled mixing in microfluidic systems using bacterial chemotaxis," Anal. Chem. **79**, 955 (2007).
[25]M. J. Kim and K. S. Breuer, "Microfluidic pump powered by setf-organizing bacteria," Small **4**, 111 (2008).
[26]A. Sokolov, I. S. Aranson, J. O. Kessler, and R. E. Goldstein, "Concentration dependence of the collective dynamics of swimming bacteria," Phys. Rev. Lett. **98**, 158102 (2007).
[27]E. B. Steager, J. A. Patel, C.-B. Kim, D. K. Yi, W. Lee, and M. J. Kim, "A novel method of microfabrication and manipulation of bacterial teamsters in low Reynolds number fluidic environments," Microfluid. Nanofluid. **5**, 337 (2008).
[28]I. S. Aranson, A. Sokolov, J. O. Kessler, and R. E. Goldstein, "Model for dynamical coherence in thin films of self-propelled microorganisms," Phys. Rev. E **75**, 040901 (2007).
[29]D. Saintillan and M. J. Shelley, "Instabilities, pattern formation, and mixing in active suspensions," Phys. Fluids **20**, 123304 (2008).
[30]D. Saintillan and M. J. Shelley, "Instabilities and pattern formation in active particle suspensions: Kinetic theory and continuum simulations," Phys. Rev. Lett. **100**, 178103 (2008).
[31]P. T. Underhill, J. P. Hernandez-Ortiz, and M. D. Graham, "Diffusion and spatial correlations in suspensions of swimming particles," Phys. Rev. Lett. **100**, 248101 (2008).
[32]J. P. Hernandez-Ortiz, P. T. Underhill, and M. D. Graham, "Dynamics of confined suspensions of swimming particules," J. Phys.: Condens. Matter **21**, 204107 (2009).
[33]J. Gray, *Animal Locomotion. The World Naturalist* (Norton, New York, 1968).
[34]J. Gray and H. W. Lissmann, "The locomotion of nematodes," J. Exp. Biol. **41**, 135 (1964).
[35]S. Brenner, "Genetics of caenorhabditis-elegans," Genetics **77**, 71 (1974).
[36]C. Elegans Sequencing Consortium, "Genome sequence of the nematode C-elegans: A platform for investigating biology," Science **282**, 2012 (1998).
[37]J. Sznitman, X. Shen, P. K. Purohit, and P. E. Arratia, "The effects of fluid viscosity on the kinematics and material properties of C. elegans swimming at low Reynolds number," Exp. Mech. **50**, 1303 (2010).
[38]J. Sznitman, P. K. Purohit, P. Krajacic, T. Lamitina, and P. E. Arratia, "Material properties of caenorhabditis elegans swimming at low Reynolds number," Biophys. J. **98**, 617 (2010).
[39]W. K. Pratt, *Digital Image Processing*, 2nd ed. (Wiley, New York, 1991).
[40]X. C. He and N. H. C. Yung, "Curvature scale space corner detector with adaptive threshold and dynamic region of support," IEEE Proceedings of the 17th International Conference on Pattern Recognition (ICPR'04), 2004, Vol. 2, pp. 791–794.
[41]C. Andrieu, N. de Freitas, A. Doucet, and M. I. Jordan, "An introduction to MCMC for machine learning," Mach. Learn. **50**, 5 (2003).
[42]N. Tavernarakis, W. Schreffler, S. Wang, and M. Driscoll, "unc-8, a DEG/ENaC family member, encodes a subunit of a candidate mechanically gated channel that modulates C-elegans locomotion," Neuron **18**, 107 (1997).
[43]J. G. Santiago, S. T. Wereley, C. D. Meinhart, D. J. Beebe, and R. J. Adrian, "A particle image velocimetry system for microfluidics," Exp. Fluids **25**, 316 (1998).
[44]J. Karbowski, C. J. Cronin, A. Seah, J. E. Mendel, D. Cleary, and P. W. Sternberg, "Conservation rules, their breakdown, and optimality in Caenorhabditis sinusoidal locomotion," J. Theor. Biol. **242**, 652 (2006).
[45]J. Korta, D. A. Clark, C. V. Gabel, L. Mahadevan, and A. D. Samuel, "Mechanosensation and mechanical load modulate the locomotory gait of swimming C-elegans," J. Exp. Biol. **210**, 2383 (2007).
[46]J. T. Pierce-Shimomura, B. L. Chen, J. J. Mun, R. Ho, R. Sarkis, and S. L. McIntire, "Genetic analysis of crawling and swimming locomotory patterns in C. elegans," Proc. Natl. Acad. Sci. U.S.A. **105**, 20982 (2008).
[47]D. F. Katz, J. R. Blake, and S. L. Paverifontana, "On the movement of slender bodies near plane boundaries at low Reynolds-number," J. Fluid Mech. **72**, 529 (1975).
[48]J. Lighthill, "Flagellar hydrodynamics," SIAM Rev. **18**, 161 (1976).
[49]E. O. Tuck, "A note on a swimming problem," J. Fluid Mech. **31**, 305 (1968).
[50]J. C. Doll, N. Harjee, N. Klejwa, R. Kwon, S. M. Coulthard, B. Petzold, M. B. Goodman, and B. L. Pruitt, "SU-8 force sensing pillar arrays for biological measurements," Lab Chip **9**, 1449 (2009).